This is the accepted manuscript made available via CHORUS. The article has been published as:

Vibrational Properties of a Monolayer Silicene Sheet Studied by Tip-Enhanced Raman Spectroscopy

Shaoxiang Sheng, Jiang-bin Wu, Xin Cong, Wenbin Li, Jian Gou, Qing Zhong, Peng Cheng, Ping-heng Tan, Lan Chen, and Kehui Wu

Phys. Rev. Lett. **119**, 196803 — Published 8 November 2017

DOI: 10.1103/PhysRevLett.119.196803

Vibrational properties of monolayer silicene sheet studied by tip-enhanced Raman spectroscopy

Shaoxiang Sheng[1], Jiang-bin Wu[2], Xin Cong[2], Wenbin Li[1], Jian Gou[1], Qing Zhong[1], Peng Cheng[1], Ping-heng Tan[2,3+], Lan Chen[1], Kehui Wu[1,3,4*]

[1]*Institute of Physics, Chinese Academy of Sciences, Beijing 100190, China*

[2] *State Key Laboratory of Superlattices and Microstructures, Institute of Semiconductors, Chinese Academy of Sciences, Beijing 100083, China*

[3] *School of physical sciences, and College of Materials Science and Opto-Electronic Technology, University of Chinese Academy of Sciences, Beijing 100049, China*

[4]*Collaborative Innovation Center of Quantum Matter, Beijing 100871, China*

[+] email: phtan@semi.ac.cn

*email：khwu@iphy.ac.cn

Abstract:

Combining ultrahigh sensitivity, spatial resolution and capability to resolve chemical information, tip-enhanced Raman spectroscopy (TERS) is a powerful tool to study molecules or nanoscale objects. Here we show that TERS can also be a powerful tool in studying two-dimensional (2D) materials. We have achieved a 10^9 Raman signal enhancement and a 0.5 nm spatial resolution using monolayer silicene on Ag(111) as a prototypical 2D material system. Due to the selective enhancement on Raman modes with vertical vibrational components in TERS, our experiment provides a direct evidence of the origination of Raman modes in silicene. Furthermore, the ultrahigh sensitivity of TERS allow us to identify different vibrational properties of silicene phases, which differ only in the bucking direction of the Si-Si bonds. Local vibrational features from defects and domain boundaries in silicene can also be identified.

Introduction

Silicene is a two-dimensional (2D) honeycomb lattice consists of silicon atoms, which can be regarded as the silicon version of graphene. As a 2D allotrope of silicon, it is fundamentally

different from bulk silicon crystals in structure and properties. The electronic band structure of silicene hosts Dirac fermions [1-3], giving rise to theoretically predicted quantum spin Hall effect and possible spintronic applications, which are of great interest to the silicon industry [4, 5]. The structures and electronic proprieties of silicene have been extensively studied by in the last few years. However, the vibrational properties of silicene still remains largely elusive, partially because *ex-situ* optical spectroscopy characterizations are hampered by the oxidation of silicene in ambient condition. So far, only a few *in-situ* Raman spectroscopy studies have been reported [6-8]. These measurements, however, failed to distinguish different phases of silicene when they coexist on the surface. In addition, as the integration of Raman spectroscopy into ultrahigh-vacuum (UHV) system usually results in low efficiency, the spectroscopy quality remains to be improved.

Compared with normal Raman, scanning tunneling microscopy (STM) with tip-enhanced Raman spectroscopy (TERS) utilizes the atomically sharp STM tip to enhance the Raman signal. The signal enhancement factor can be as high as 10^8 [9]. Moreover, TERS is capable to access the local surface atomic structure and chemical information simultaneously. Recently, improvements in the spatial resolution, down to sub-nanometer scale, have been demonstrated in the "gap-mode" (both tip and substrate are plasmonic metals, such as Au/Ag) TERS on carbon nanotubes[9] and molecules on Ag(111) surfaces[10, 11]. With such a high spatial resolution, it is possible to study the local vibrational properties of silicene *in-situ* in ultrahigh vacuum.

In the present work, we demonstrate a high-performance TERS spectroscopy based on a UHV low-temperature STM system. A signal enhancement factor as high as 10^9 and a TERS spatial resolution of 0.5 nm have been achieved by using silicene on Ag(111) as a prototypical system. As such, we were able to distinguish the vibrational signatures of different monolayer silicene phases, which are different only in the buckling direction of the Si-Si bonds. Moreover, the TERS enhancement is phonon mode-selective, which helps us to clarify the origins of the Raman peaks of silicene. The sub-nanometer spatial resolution also makes it possible to distinguish the Raman signatures from defects and domain boundaries in silicene. This work paves the way to employ TERS as a universal, high-sensitive local tool to study emerging new 2D materials.

Method

Our TERS is built in a homemade LT-UHV STM system, with side illumination and backscattering collection configuration, as shown in Fig. 1(a). The aspheric lens (NA=0.42, f=24 mm, diameter=25 mm) inside the STM body can be adjusted by a 3D piezoelectric motor. The Ag(111) surface was prepared by standard cycles of argon ion sputtering and annealing at about 800 K. Silicene was prepared by heating a Si wafer piece (T ~ 1300 K) to evaporate Si onto the Ag(111). The substrate was held at 460 K for preparing 4×4 / $\sqrt{13}\times\sqrt{13}$ phase, and 500 K for $2\sqrt{3}\times2\sqrt{3}$ phase. The Ag tip was chemically etched, and cleaned by heating at around 900 K in ultra-high vacuum, and further modified by in-situ voltage pulses on a clean Ag surface for TERS measurements and STM imaging. A single longitudinal mode fiber coupled CW laser (Cobolt, Sweden) was used to provide a p-polarized laser light as the Raman pumping source, with the wavelength at 532 nm and a photon flux about 10 kW/cm^2. The scattered Raman signals were dispersed by a 1200 grooves/mm grating and collected by a liquid nitrogen cooled charge coupled device (CCD) (Princeton Instrument, SP2300i). All TERS experiments were carried out at sample temperature of 77 K, and a base pressure around 2×10^{-10} mbar.

The phonon spectra and vibrational density of states (VDOS) were calculated using density functional perturbation theory (DFPT) implemented in the Quantum Espresso code [12]. For the calculation of the phonon dispersion of silicene on Ag(111), VASP[13] and PHON[14] were used, with exchange-correlation potential described by the PBE function [15]. The cutoff energy of the plane wave was 360 eV, and Monkhorst-Pack[15] reciprocal grids is 12×12×1. The structure of (3×3) and $\sqrt{7}\times\sqrt{7}$ silicene supercells are relaxed on a 5 layers Ag(111) substrate. In the phonon dispersion calculation by PHON, only the silicene part was considered, by using the same isolated method in ref. 6. A (2×2) supercell was adopted to perfect the accuracy.

Results and discussions:

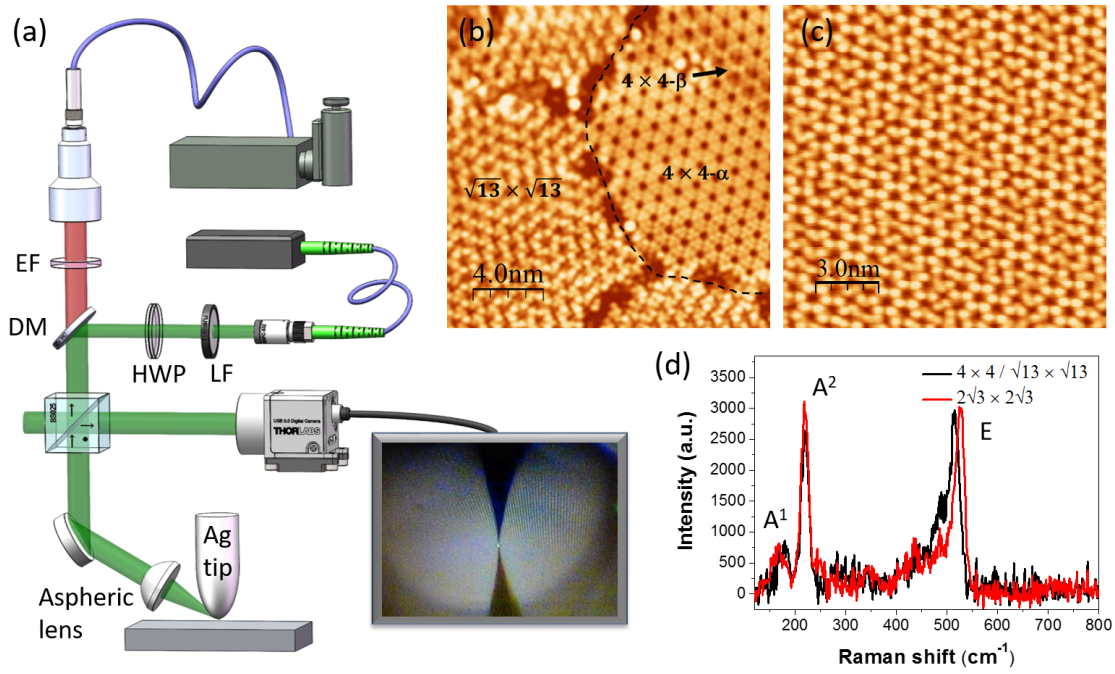

Fig. 1. The experimental setup. (a) Schematic of LT-UHV STM based TERS setup. EF: edge filter, DM: dichroic mirror, HWP: half wave plate, LF: laser line filter. (b, c) Atomic resolution STM topography of coexisted 4×4 and $\sqrt{13}\times\sqrt{13}$ ((b), 0.2 V, 300 pA), and $2\sqrt{3}\times2\sqrt{3}$ ((c), 2 V, 50 pA) silicene phase. (d) Corresponding *in-situ* normal Raman spectra (Laser power is about 5 mW, acquisition time is 600 s).

Compared with flat C-C bonds in graphene, the Si-Si bonds in silicene exhibit various buckling configurations on Ag(111) surface, resulting in ordered phases, such as 4×4 (silicene 3×3 supercell on Ag(111) 4×4 supercell), $(\sqrt{13}\times\sqrt{13})$R13.9° (silicene $\sqrt{7}\times\sqrt{7}$ on Ag(111) $\sqrt{13}\times\sqrt{13}$) and $(2\sqrt{3}\times2\sqrt{3})$R30° (silicene $\sqrt{7}\times\sqrt{7}$ on Ag(111) $2\sqrt{3}\times2\sqrt{3}$) [16-18]. The 4×4 and $\sqrt{13}\times\sqrt{13}$ phases usually coexist (Fig. 1(b)), whereas the $2\sqrt{3}\times2\sqrt{3}$ phase can be prepared as a single phase covering the entire Ag(111) surface (Fig. 1(c))[18]. We first obtained the far field Raman spectra (without tip enhancement) for a mixed 4×4 /$\sqrt{13}\times\sqrt{13}$ surface and a pure $2\sqrt{3}\times2\sqrt{3}$ surface, respectively, as shown in Fig. 1(d). Three major peaks are presented in the spectra, which agree with the *in-situ* Raman measurement by D. Solonenko et al [6]. The peak around 520 cm^{-1} (4×4 /$\sqrt{13}\times\sqrt{13}$ at 515 cm^{-1}, and $2\sqrt{3}\times2\sqrt{3}$ at 527 cm^{-1}) is known as the E mode, corresponding to a double-degenerated modes of the in-plane transversal optical (TO) and in-plane longitudinal optical (LO) phonon branches [19]. It has been observed in both in-situ and ex-situ Raman studies [20]. The presence of the E mode reflects the honeycomb nature of 2D

silicene. The two low energy modes, at around 170 cm^{-1} and 218 cm^{-1}, are only reported by *in-situ* Raman measurements [6, 7] and are absent in *ex-situ* measurements [20]. The peak at 218 cm^{-1} was also not presented in the calculated phonon spectrum of freestanding silicene [19], it had been suggested to be Raman bands activated by defects (analogy to the so-called D band in graphene) [7]. Recently, D. Solonenko et al. determined from the polarization dependence of these peaks that they should be phonon modes with A symmetry [6]. Here, we denoted these modes as A^1 and A^2 modes following ref. 6.

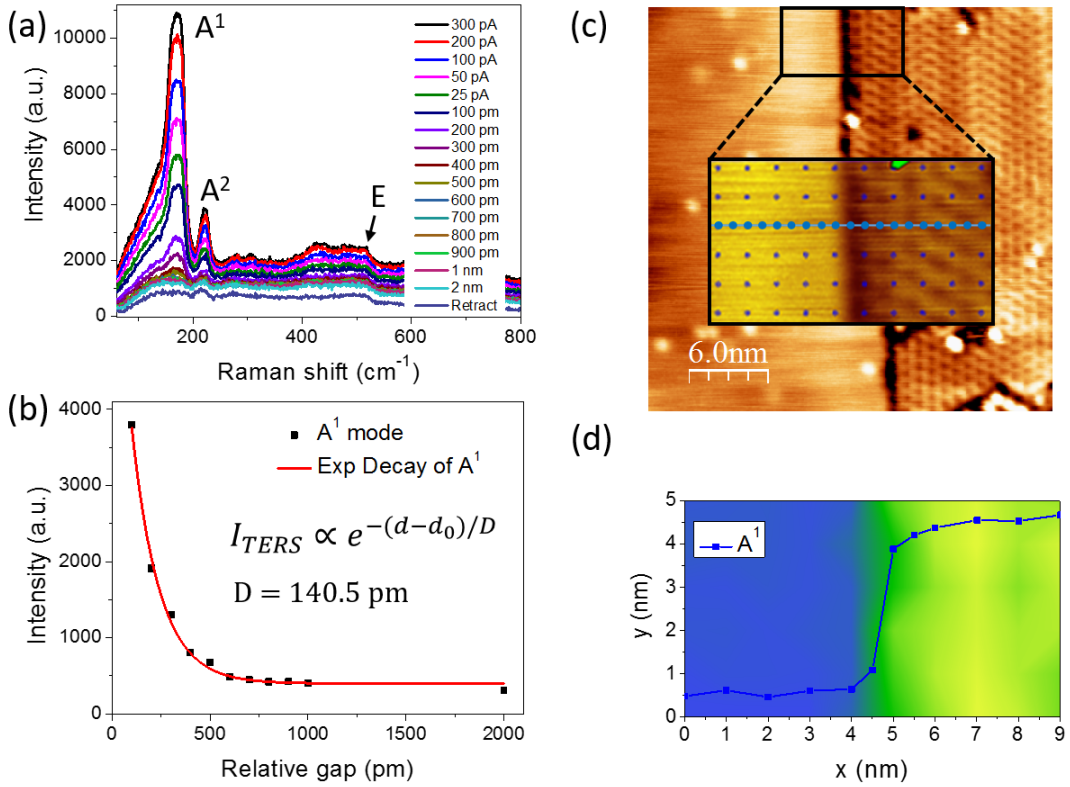

Fig. 2. Enhancement factor and spatial resolution of TERS. (a) Gap-distance dependent TERS spectra of silicene $\sqrt{13}\times\sqrt{13}$ phase (1 V, 50 s for each spectrum). (b) TERS intensity of the A^1 mode dependent on the relative gap distance (tip retracted from 100 pm to 2 nm. The TERS data with tunneling current were not used, as the tip height is difficult to acquire with feedback on). (c) STM topography of $\sqrt{13}\times\sqrt{13}$ phase on Ag(111) surface, inset is the enlarged STM image in the black box. (d) A^1 mode TERS intensity mapping of $\sqrt{13}\times\sqrt{13}$ phase on Ag(111) surface in the inset in (c), the overlapped dots line is the A^1 mode TERS intensity along the blue dot line in (c) (1V, 300 pA).

When the STM tip is brought close to the silicene surface, strong enhancement of the Raman

signal is observed, as shown in Fig 2(a). Both the A^1 and A^2 peaks exhibit dramatic tip-enhancement and become the dominant peak as the tip is close to the surface. In contrast, the E mode shows negligible enhancement and becomes insignificant when the tip is close to the surface. This phenomenon can be understood as the tip mainly enhances the vertical electric field along the tip axis, so only the out-of-plane vibrational modes are enhanced [10]. The A modes have dominating out-of-plane vibration of the Si atoms, thus they can be effectively enhanced under a local vertical electric field. In contrast, in the E mode, the displacements of Si atoms are purely in-plane, so it exhibits negligible tip-enhancement under a vertical electric field. This selection rule can be expressed by the TERS intensity of each mode, $I_{TERS,M} \propto \left|\square_{ZZ,M} \cdot g_{zz}^2\right|^2$, where g_{zz} is the ZZ component of the electric field enhancement tensor and $\alpha_{ZZ,M}$ is the ZZ component of the Raman tensor of each mode. Because both A^1 and A^2 modes have a nonzero α_{ZZ} Raman tensor[6], they can be effectively enhanced under a vertical electric field. In contrast, in the E mode, the α_{ZZ} Raman tensor is zero, so it exhibits negligible tip-enhancement. Thus, our TERS experiment provides a direct support to the assignment of the major Raman peaks of silicene at 170 cm^{-1} and 218 cm^{-1}, and 520 cm^{-1} to A^1, A^2 and E modes.

A careful calibration on the intensity of the A^1 mode as a function of the gap distance between the tip and the sample, as detailed in the supplementary materials which include Refs. [21-32], indicates that we have achieved an unprecedent TERS enhancement factor up to 10^9. The dependence of TERS intensity on the gap distance fits well with an exponential decay (Fig. 2(b)), suggesting that the TERS enhancement comes from the enhancement of the local electric field. Moreover, an extremely high TERS lateral spatial resolution were also demonstrated in the same system. As shown in Fig. 2(c), the flat area on the left side is the clean Ag surface, and the right part is silicene with $\sqrt{13}\times\sqrt{13}$ phase. TERS spectra were recorded along the blue dots line in the inset in Fig. 2(c). The color map in Fig 2(d) illustrates the chemical distribution on the surface. When the tip moves across a step, the Raman intensity (A^1 mode is used as the reference peak) follows the abrupt morphology change, giving a spectroscopic spatial resolution as high as 0.5 nm spatial resolution with a 10%-90% contrast, which is among the best record so far [10, 11]. These results show that TERS is an ideal tool for studying the local vibrational properties of silicene.

Due to the extremely high signal enhancement and spatial resolution, we were also able to resolve vibrational features that are not observable in normal Raman spectroscopy. Figure 3(a)-(c) show the gap-distance dependent TERS spectra of 4×4, $\sqrt{13}\times\sqrt{13}$, and $2\sqrt{3}\times2\sqrt{3}$ phases, respectively, obtained by placing the STM tip on top of each specific phase. In addition to the A^1, A^2 and E peaks, several additional features can be observed, including a side peak (LA) around 120 cm^{-1}, which results in the asymmetric shape of the A^1 peak, and a serials of small peaks, which can be classified into two groups, one around 300 cm^{-1} (denoted by ZO_x) and the other around 420-480 cm^{-1} (denoted by LO_x and TO), respectively. Note that these spectra were obtained locally from an effective area of ~ 1 nm size, which is guaranteed by high resolution STM images to be clean silicene phases. Therefore, we can safely rule out any contamination induced peaks, such as those from amorphous silicon [33].

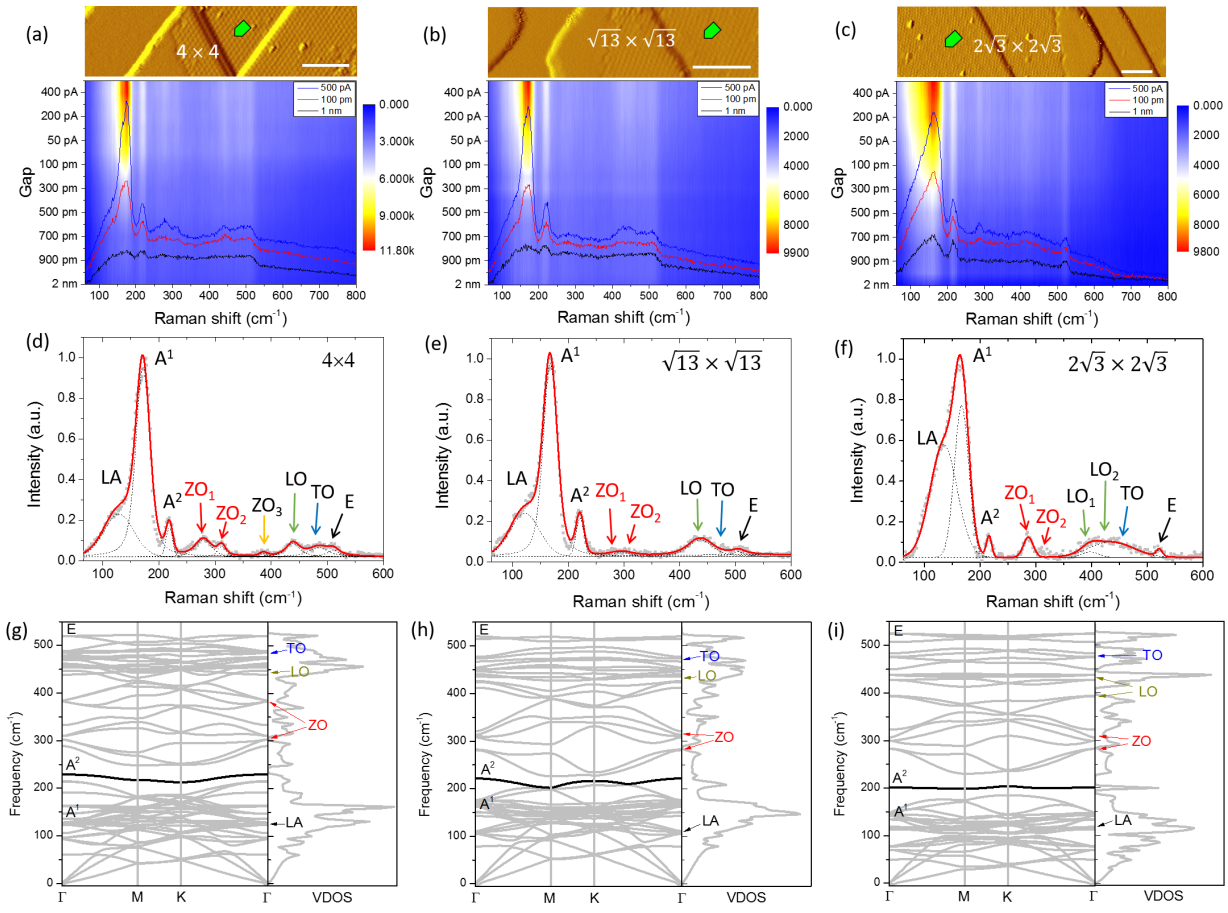

Fig. 3. Near field Raman spectra of silicene and the calculated supercells phonon dispersion curves with taking into account the effect of Ag(111) substrate. (a-c) Gap-distance dependent TERS spectra map of silicene 4×4

(a), $\sqrt{13}\times\sqrt{13}$ (b), and $2\sqrt{3}\times2\sqrt{3}$ (c) phases (1 V, 50 s), with tip position in the corresponding STM topography (upper panels, the scale bar is 10 nm). (d-f) Pure near field TERS spectra (subtracted far field signals) of silicene 4×4 (d), $\sqrt{13}\times\sqrt{13}$ (e), and $2\sqrt{3}\times2\sqrt{3}$ (f) phases. Experimental data are shown by gray crosses, and the fitting data are plotted by red solid lines. Each single mode is plotted by dash gray line. (g-i) The supercells phonon dispersion curves and VDOS of the silicene 4×4 phase (g), $\sqrt{13}\times\sqrt{13}$ phase (h), and $2\sqrt{3}\times2\sqrt{3}$ phase (i) epitaxial on Ag(111) surface.

Carefully inspecting the TERS spectra of different phases, one can notice the clear difference among them. For examples, the spectrum of $2\sqrt{3}\times2\sqrt{3}$ phase has a much higher LA band, resulting in an apparently fatter A^1 peak. This may be explained by the fact the $2\sqrt{3}\times2\sqrt{3}$ phase is more disordered, and thus the Raman selection rules are more relaxed, allowing a more effective excitation of the LA band. In addition, $2\sqrt{3}\times2\sqrt{3}$ phase also exhibits a broader LO-TO band, i.e. LO-TO peaks are more split. In contrast, the ZO band is stronger and more split in the spectrum of 4x4 phase, while it is weaker in the spectrum of $2\sqrt{3}\times2\sqrt{3}$ phase, and only slightly visible in the spectrum of $\sqrt{13}\times\sqrt{13}$ phase.

These additional peak features, however, cannot be explained without considering the substrate effect. In the calculated phonon spectra of free-standing silicene with 3x3 and $\sqrt{7}\times\sqrt{7}$ reconstructions (with respect to silicene 1x1, corresponding to 4x4 and $2\sqrt{3}\times2\sqrt{3}$ phases on Ag(111)), ZO and LO(TO) bands are presented in the Brillouin zone center due to phonon folding in the supercell, but their energies are degenerated at the Γ point, therefore both ZO and LO should exhibit only single narrow peaks. In order to reproduce the multiple peaks in the ZO and LO bands, we included the Ag(111) substrate in the calculation, as shown in Fig 3(g)-(i). The degenerated ZO, LO(TO) modes are found to split to multiple phonon branches at the Γ point, agreeing well with our experiment. Furthermore, the differences in the ZO and LO-TO groups in different silicene phases can also be perfectly reproduced in the calculated phonon spectra. Firstly, in the measured spectrum of $2\sqrt{3}\times2\sqrt{3}$ phase, the LO mode is clearly red-shift and split at ~395 cm^{-1} (LO_1) and 426 cm^{-1} (LO_2), whereas the LO-TO bands in 4x4 and $\sqrt{13}\times\sqrt{13}$ are located in a narrower energy region , more close to the E mode at 520 cm^{-1}. These features are

perfectly reproduced in the calculations. On the other hand, the 4x4 phase exhibits apparently difference ZO group compared with those of $2\sqrt{3}\times2\sqrt{3}$ and $\sqrt{13}\times\sqrt{13}$ phases. There is a peak at ~380 cm^{-1} (ZO_3) of 4×4 phase (Fig. 3(d)), which is absent in $\sqrt{13}\times\sqrt{13}$ and $2\sqrt{3}\times2\sqrt{3}$ phases (Fig. 3(e, f)). In the calculated phonon spectrum (Fig. 3(g)), a ZO phonon branch reaches exactly this energy at the Γ point, which is absent in the phonon spectra of $2\sqrt{3}\times2\sqrt{3}$ and $\sqrt{13}\times\sqrt{13}$ phases (Fig. 3(h-i)). The atomic vibrational pictures of each Raman modes are all summarized in Table S1. Note that the low frequencies modes of LA, A^1 and A^2 have large out-of-plane vibration components, which explains their large TERS enhancement. On the other hand, the ZO, LO and TO modes have much smaller out-of-plane components, correspondingly their TERS enhancements are much less significant. Note that the A^2 peak can also be attributed to one phonon branch at Γ point which possesses the narrowest peak width, agreeing with our experiment (Fig. 3(a-c)) and ref. 6. Overall, the TERS results match the calculations well when take into account the effect of Ag(111) substrate.

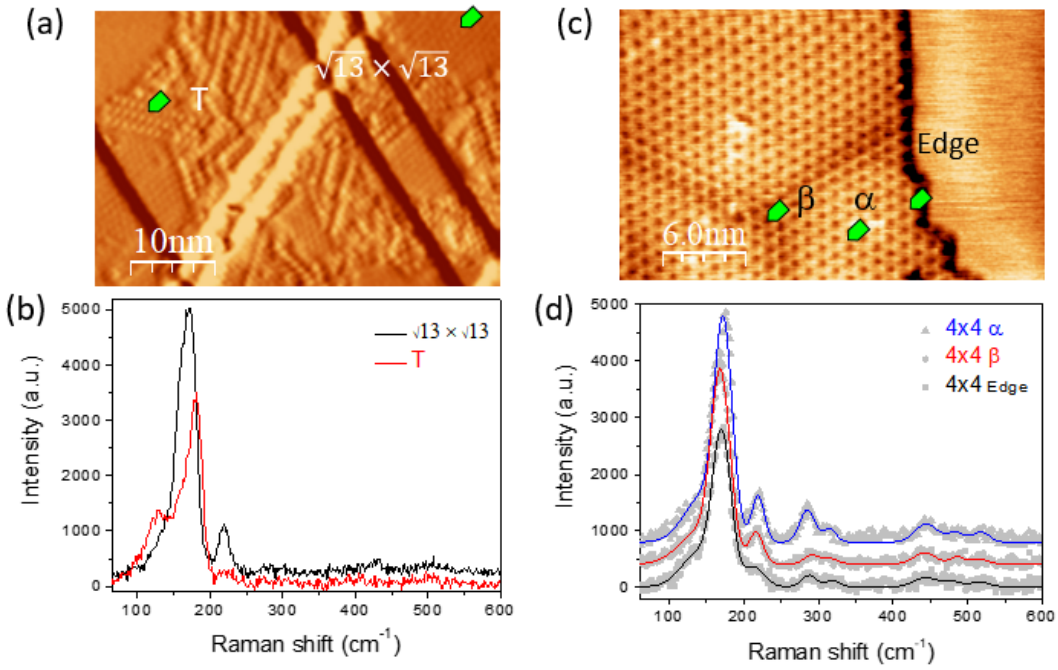

Fig. 4. TERS spectra of silicene at defect, edge and local strain positions. (a) STM topography of coexisting silicene T phase and $\sqrt{13}\times\sqrt{13}$ phase. (b) TERS spectra of T phase and well-ordered $\sqrt{13}\times\sqrt{13}$ phase, with the tip at the corresponding position marked in (a) (1 V, 100 pA), shows very different spectra. (c) STM topography of silicene 4×4-α phase and β phase. (d) TERS spectra at 4×4-α phase, β phase, and domain edge,

with the tip at the corresponding position in (c) (1 V, 50 pA). The far field signal has been subtracted from all of the TERS spectra, the acquisition time is 50 s, and the laser power is about 10 mW.

Finally, the ultrahigh sensitivity of TERS also allows us to study the local vibrational properties induced by defects or domain boundaries in silicene, as it has been used to characterize nanostructured materials like carbon nanotubes (CNTs) [9, 34, 35] and graphene [36, 37]. The silicene T phase was rarely discussed in literature. It was likely a partially disordered phase consists incomplete silicon rings [18], and also suggested to be another type of $\sqrt{13}\times\sqrt{13}$ phase [16]. Here, our TERS results indicate significant differences between the TERS spectra of T phase compared with those from other ordered silicene phases, as shown in Fig. 4(a). It exhibits a blue shift of A^1 peak, and with a strong shoulder peak at 130 cm^{-1}. The A^2 peak is almost absent in T phase. It maybe because the relaxation of the Raman selection rule for LA mode due to the disorder of the silicon rings, and the A^2 mode is suppressed due to a very different silicene-Ag interaction as compared with other ordered phases.

It is known that another phase with a 4×4 periodicity, namely 4×4-β phase, commonly exists at the boundary between different normal 4×4 domains (noted as 4×4-α phase) [38, 39]. The strain effect helps to stabilize the 4×4-β phase. The TERS spectra taken on 4×4-α region and at the boundary (β phases) show clear differences. As shown in Fig. 4(d), the β phase shows a slight red shift (~ 4 cm^{-1}) of the A^1 mode and a much lower peak at ZO peaks (280 cm^{-1} and 310 cm^{-1}) compared with α phase. The TERS spectrum at the edge of a 4×4-α domain was also measured, and its A^1 and A^2 peaks are similar like those of the 4×4-β phase but with an even lower intensity. Considering that the A^2 peak and the ZO peaks are directly related to the interaction between silicene and the substrate, the decreasing A^2 and ZO peak intensity from α, β to edge may imply decreasing interaction with the substrate due to strain relaxation at the domain boundary and domain edge, respectively.

In summary, we have demonstrated TERS with enhancement factor as high as 10^9, and spatial resolution of 0.5 nm using a 2D material silicene on Ag(111) as a model system. The vibrational fingerprints of different silicene phases, which differ only in the buckling direction of the Si-Si chemical bonds, can be distinguished in TERS spectra. In addition we have revealed ZO, LO and

TO phonon modes at high frequencies, which were not observable in normal Raman. We show that beyond molecules, TERS can also play powerful roles in studying 2D materials, such as defects, domain boundaries, and local strains. The highly enhanced field perpendicular to the surface makes TERS a selective-modes enhancement behavior, and may also be a useful tool to tune the properties of 2D materials, such as to open an energy gap at K-points [4, 5] of silicene energy bands, which is potentially useful for the light controlled logic circuit.

Acknowledgments:

This work was supported by, MOST of China (2016YFA0300904, 2016YFA0301204), NSF of China (Grants No. 11334011, 11474277, 11434010, 11225421) and the Strategic Priority Research Program of the Chinese Academy of Sciences, Grants No. XDB07020100 and XDB01020303.

References

[1] B.J. Feng, H. Li, C.C. Liu, T.N. Shao, P. Cheng, Y.G. Yao, S. Meng, L. Chen, K.H. Wu, Acs Nano **7**, 9049 (2013).
[2] L. Chen, H. Li, B. Feng, Z. Ding, J. Qiu, P. Cheng, K. Wu, S. Meng, Phys. Rev. Lett. **110**, 085504 (2013).
[3] Y. Feng, D.F. Liu, B.J. Feng, X. Liu, L. Zhao, Z.J. Xie, Y. Liu, A.J. Liang, C. Hu, Y. Hu, S.L. He, G.D. Liu, J. Zhang, C.T. Chen, Z.Y. Xu, L. Chen, K.H. Wu, Y.T. Liu, H. Lin, Z.Q. Huang, C.H. Hsu, F.C. Chuang, A. Bansil, X.J. Zhou, Proc. Natl Acad. Sci. USA **113**, 14656 (2016).
[4] L. Tao, E. Cinquanta, D. Chiappe, C. Grazianetti, M. Fanciulli, M. Dubey, A. Molle, D. Akinwande, Nat. Nanotech. **10**, 227 (2015).
[5] W.F. Tsai, C.Y. Huang, T.R. Chang, H. Lin, H.T. Jeng, A. Bansil, Nat. Commun. **4**, 1500 (2013).
[6] D. Solonenko, O.D. Gordan, G.L. Lay, H. Şahin, S. Cahangirov, D.R.T. Zahn, P. Vogt, 2D Mater. **4**, 015008 (2016).
[7] J.C. Zhuang, X. Xu, Y. Du, K. Wu, L. Chen, W. Hao, J. Wang, W.K. Yeoh, X. Wang, S.X. Dou, Phys. Rev. B **91**, 161409 (2015).
[8] A. Díaz Álvarez, T. Zhu, J.P. Nys, M. Berthe, M. Empis, J. Schreiber, B. Grandidier, T. Xu, Surf. Sci. **653**, 92 (2016).
[9] M. Liao, S. Jiang, C. Hu, R. Zhang, Y. Kuang, J. Zhu, Y. Zhang, Z. Dong, Nano Lett. **16**, 4040 (2016).
[10] R. Zhang, Y. Zhang, Z.C. Dong, S. Jiang, C. Zhang, L.G. Chen, L. Zhang, Y. Liao, J. Aizpurua, Y. Luo, J.L. Yang, J.G. Hou, Nature **498**, 82 (2013).
[11] S. Jiang, Y. Zhang, R. Zhang, C. Hu, M. Liao, Y. Luo, J. Yang, Z. Dong, J.G. Hou, Nat. Nanotech. **10**, 865 (2015).
[12] S. Baroni, S. de Gironcoli, A. Dal Corso, P. Giannozzi, Rev. Mod. Phys. **73**, 515 (2001).
[13] G. Kresse, J. Hafner, Phys. Rev. B **47**, 558 (1993).
[14] D. Alfè, Comput. Phys. Commun. **180**, 2622 (2009).
[15] H.J. Monkhorst, J.D. Pack, Phys. Rev. B **13**, 5188 (1976).
[16] D. Chiappe, C. Grazianetti, G. Tallarida, M. Fanciulli, A. Molle, Adv. Mater. **24**, 5088 (2012).
[17] P. Vogt, P. De Padova, C. Quaresima, J. Avila, E. Frantzeskakis, M.C. Asensio, A. Resta, B. Ealet, G. Le Lay, Phys. Rev. Lett. **108**, 155501 (2012).
[18] B.J. Feng, Z. Ding, S. Meng, Y. Yao, X. He, P. Cheng, L. Chen, K. Wu, Nano Lett. **12**, 3507 (2012).
[19] E. Scalise, M. Houssa, G. Pourtois, B. van den Broek, V. Afanas'ev, A. Stesmans, Nano Res. **6**, 19 (2013).

[20] E. Cinquanta, E. Scalise, D. Chiappe, C. Grazianetti, B. van den Broek, M. Houssa, M. Fanciulli, A. Molle, J. Phys. Chem. C **117**, 16719 (2013).
[21] B. Pettinger, B. Ren, G. Picardi, R. Schuster, G. Ertl, Phys. Rev. Lett. **92**, 096101 (2004).
[22] N. Jiang, E.T. Foley, J.M. Klingsporn, M.D. Sonntag, N.A. Valley, J.A. Dieringer, T. Seideman, G.C. Schatz, M.C. Hersam, R.P. Van Duyne, Nano Lett. **12**, 5061 (2012).
[23] B. Pettinger, P. Schambach, C.J. Villagomez, N. Scott, Annu. Rev. Phys. Chem. **63**, 379 (2012).
[24] J. Steidtner, B. Pettinger, Phys. Rev. Lett. **100**, 236101 (2008).
[25] J. Stadler, T. Schmid, R. Zenobi, Nano Lett. **10**, 4514 (2010).
[26] J. Stadler, T. Schmid, R. Zenobi, Nanoscale **4**, 1856 (2012).
[27] H.K. Wickramasinghe, M. Chaigneau, R. Yasukuni, G. Picardi, R. Ossikovski, Acs Nano **8**, 3421 (2014).
[28] K.F. Domke, D. Zhang, B. Pettinger, J. Am. Chem. Soc. **128**, 14721 (2006).
[29] R.M. Stockle, Y.D. Suh, V. Deckert, R. Zenobi, Chem. Phys. Lett. **318**, 131 (2000).
[30] E.D. Palik, Handbook of optical constants of solids, Academic Press, Orlando, 1985.
[31] N.L. Gruenke, M.F. Cardinal, M.O. McAnally, R.R. Frontiera, G.C. Schatz, R.P. Van Duyne, Chem. Soc. Rev. **45**, 2263 (2016).
[32] P. Kukura, D.W. McCamant, R.A. Mathies, Annu. Rev. Phys. Chem. **58**, 461 (2007).
[33] D. Solonenko, O.D. Gordan, G. Le Lay, D.R.T. Zahn, P. Vogt, Beilstein J. Nanotech. **8**, 1357 (2017).
[34] Y. Okuno, Y. Saito, S. Kawata, P. Verma, Phys. Rev. Lett. **111**, 216101 (2013).
[35] T.A. Yano, T. Ichimura, S. Kuwahara, F. H'Dhili, K. Uetsuki, Y. Okuno, P. Verma, S. Kawata, Nat. Commun. **4**, 2592 (2013).
[36] R. Beams, L.G. Cancado, A. Jorio, A.N. Vamivakas, L. Novotny, Nanotechnology **26**, 175702 (2015).
[37] K.D. Park, M.B. Raschke, J.M. Atkin, Y.H. Lee, M.S. Jeong, Adv. Mater. **29**, (2017).
[38] J.L. Qiu, H. Fu, Y. Xu, A.I. Oreshkin, T. Shao, H. Li, S. Meng, L. Chen, K. Wu, Phys. Rev. Lett. **114**, 126101 (2015).
[39] W.B. Li, S.X. Sheng, J. Chen, P. Cheng, L. Chen, K. Wu, Phys. Rev. B **93**, (2016).